



# Crystallization Characteristics and Properties of Glass Ceramics Derived from Iron Tailing

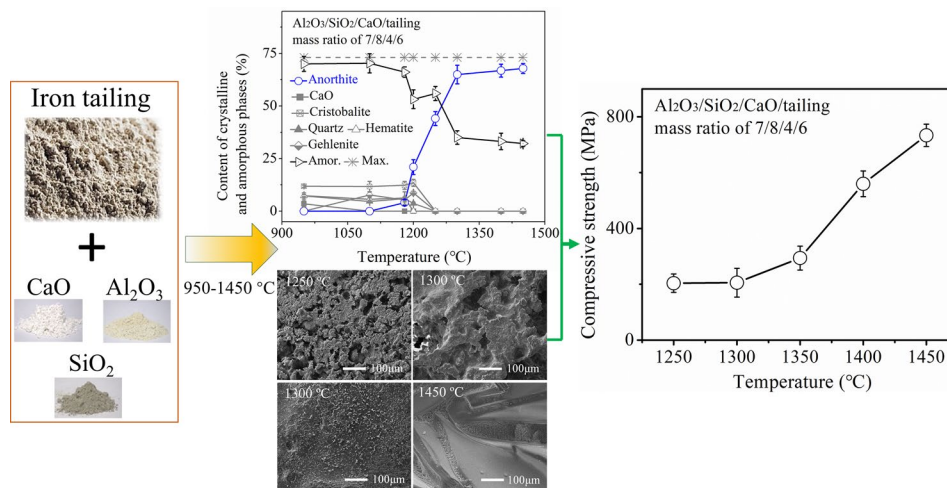
Xingwen Lu<sup>1</sup> · Ceng Zhou<sup>1</sup> · Yuxin Liu<sup>1</sup> · Yujie Wang<sup>1</sup> · Fei Wang<sup>2</sup>

Received: 13 January 2022 / Accepted: 30 May 2022  
© The Minerals, Metals & Materials Society 2022

## Abstract

In this study, iron tailings were used as raw materials mixing with  $\text{Al}_2\text{O}_3$ ,  $\text{SiO}_2$ , and/or  $\text{CaO}$  sintered at 950–1400 °C to produce glass ceramics. In  $\text{Al}_2\text{O}_3$ /tailing and  $\text{Al}_2\text{O}_3$ / $\text{SiO}_2$ /tailing systems, the newly formed crystalline mullite ( $3\text{Al}_2\text{O}_3 \cdot 2\text{SiO}_2$ ) reached its maximum content of 83.7 wt% for sample with  $\text{Al}_2\text{O}_3$ / $\text{SiO}_2$ /tailing mass ratio of 6/2/2. In  $\text{Al}_2\text{O}_3$ / $\text{SiO}_2$ / $\text{CaO}$ /tailing system, the content of newly formed anorthite ( $\text{CaAl}_2\text{Si}_2\text{O}_8$ ) increased to the maximum of 72.9 wt% for sample with  $\text{Al}_2\text{O}_3$ / $\text{SiO}_2$ / $\text{CaO}$ /tailing mass ratio of 7/8/4/6 sintered at 1450 °C. The properties of glass ceramic products were significantly improved in samples with high content of crystalline mullite or anorthite and low surface porosity. Obtained glass ceramic in  $\text{Al}_2\text{O}_3$ / $\text{SiO}_2$ /tailing system with mass ratio of 6/2/6 showed excellent properties of chemical resistance (99.99%), compressive strength (1061.6 MPa), and low water absorption (0.2%). The high performance of glass ceramics and low leachability of hazardous metals shed light on the potential application of iron tailings in building and decorative materials.

## Graphical Abstract



**Keywords** Glass ceramic · Iron tailings · Properties · Crystal transformation · Quantitative X-ray diffraction

## Introduction

With the rising development of steel industry, large amount of iron tailings is generated in recent decades. In 2013, the total amount of iron tailings was reported to be over 5 billion tons in China [1], and the amount is keeping increasing at 5.5 million tons yearly [2]. These iron

The contributing editor for this article was João António Labrincha Batista.

✉ Fei Wang  
feiwang1984@gmail.com

Extended author information available on the last page of the article

tailings were usually disposed in tailings dams, which not only occupies large area of landfill sites [3] but also causes serious pollution to around environment, due to the easily release of hazardous metals in iron tailings into soil, river, and underground water [4]. However, iron tailings consist of useful elements, such as, silica, alumina, and iron oxide (Weishi et al. 2018), which make iron tailings to generate construction materials to meet the increasing demand for building industry.

Previous studies have showed that iron tailings can be effectively utilized as raw materials to produce construction materials, such as, cement [5], refractory [6], concrete aggregate [1, 7, 8], bricks [9], ceramsite [10–12], and glass ceramics [13]. Among these materials, tailings-based glass ceramics were considered with excellent mechanical and chemical properties for building and engineering applications [9, 14, 15]. Furthermore, the transformation of iron tailings into glass ceramics can insert hazardous metals into a multi crystalline matrix to reduce their leachability. Thus, converting iron tailings into glass ceramics will provide an avenue for converting iron tailing into glass ceramic products to reduce its environmental hazard. Many studies had reported the effects of initial composition [16–18], nucleating agents [14, 19, 20], and heat treatment conditions [21, 22] on the mechanical and chemical properties of the obtained glass ceramic products.

However, crystallization behavior of desirable phases should be reasonably controlled to obtain glass ceramic products with specific microstructure and properties. Effect of sintering on the properties of the iron tailing-based glass ceramics along with crystallization has not been studied thoroughly in the literature. As glass ceramics are polycrystalline materials prepared by crystallization processes [23], the quantitative understanding of crystalline transformation under thermal conditions is essential for determining the properties of glass ceramic products. In addition, the influence of phase transformation on properties of ceramic membrane needs to be distinguished to find out iron tailing-based glass ceramics with desirable properties.

In this study, a series of glass ceramic products were prepared by sintering iron tailings with the addition of  $\text{Al}_2\text{O}_3$ ,  $\text{SiO}_2$ , and  $\text{CaO}$ . Microstructure, phase composition, mechanical, and chemical properties of the products were systematically investigated in terms of initial material composition and heat treatment condition. Phase transformation and crystallization in sintering process were detailed and examined to clarify its effect on the microstructure and properties of glass ceramic products. Finally, prolonged toxicity leaching test was examined to determine the leachability of Pb, Zn, Cu, Cr, and Ni in the sintered products for the safe usage of the products.

## Experimental Procedures

### Raw Materials

Iron tailings used in this work were collected from Daboshan Mining Co., Ltd (Shaoguan, Guangdong, China). The chemicals of alumina ( $\text{Al}_2\text{O}_3$ , 99.99%), silicon dioxide ( $\text{SiO}_2$ , 99.9%), and calcium oxide ( $\text{CaO}$ , 98%) were purchased from Aladdin Co., Ltd. In addition, the particle sizes of alumina, silicon dioxide, and calcium oxide were measured by a Malvern Mastersizer fitted with a Hydro 2000MU dispersion unit (Worcestershire, UK). The obtained medium sizes of alumina, silicon dioxide, and calcium oxide were 20.23  $\mu\text{m}$ , 4.446  $\mu\text{m}$ , and 10.27  $\mu\text{m}$ , respectively. Calcium fluoride ( $\text{CaF}_2$ , 99.99%) was purchased from Sigma-Aldrich (St. Louis, MO). Iron tailings, alumina, silicon dioxide, and calcium oxide were dried at 105 °C for 48 h to remove the moisture. The dried iron tailings were then grounded into powder with particle size less than 75  $\mu\text{m}$  by ball milling.

The main chemical composition of iron tailings was examined by energy-dispersive X-ray fluorescence spectroscopy (XRF, EDX-7000P, Shimadzu, China) to be  $\text{Fe}_2\text{O}_3$  (45.25%),  $\text{SiO}_2$  (27.1%),  $\text{Al}_2\text{O}_3$  (14.27%),  $\text{CaO}$  (1.18%),  $\text{MgO}$  (0.69%),  $\text{K}_2\text{O}$  (1.56%),  $\text{CuO}$  (0.75%),  $\text{ZnO}$  (0.67%),  $\text{PbO}$  (0.42%),  $\text{MnO}$  (0.30%), and others (7.81%). The main minerals in iron tailings were identified by X-ray diffraction (XRD, Empyrean, panalytical, The Netherlands), with reference to the Powder Diffraction File (PDF) database published by the International Centre for Diffraction Data (ICDD), as a mixture of the quartz ( $\text{SiO}_2$ , PDF #85-0797), hematite ( $\text{Fe}_2\text{O}_3$ , PDF #89-0597), mayenite ( $(\text{CaO})_{12}(\text{Al}_2\text{O}_3)_7$ , PDF #70-2144), and braunite ( $(\text{Mn}_2\text{O}_3)_3\text{MnSiO}_3$ , PDF #74-1206) [Supplementary Information (SI) of Figure S1]. Alumina, silicon dioxide, and calcium oxide powder were identified by XRD as a single-phase sample, which matched the standard peaks of aluminum oxide (PDF #50-0741), cristobalite (PDF #77-1316), and lime (PDF #99-0070).

### Sample Preparation

$\text{Al}_2\text{O}_3$ ,  $\text{SiO}_2$ , and  $\text{CaO}$  were mixed with iron tailings at different mass ratios (Table 1), and the corresponding

**Table 1** Mass ratios of  $\text{Al}_2\text{O}_3$ /tailing,  $\text{Al}_2\text{O}_3/\text{SiO}_2$ /tailing and  $\text{Al}_2\text{O}_3/\text{SiO}_2/\text{CaO}$ /tailing used for the sintered samples

Sample no.	Mass ratios of $\text{Al}_2\text{O}_3$ /tailing	Mass ratios of $\text{Al}_2\text{O}_3/\text{SiO}_2$ /tailing	Mass ratios of $\text{Al}_2\text{O}_3/\text{SiO}_2/\text{CaO}$ /tailing
1	2/2	6/2/1	7/8/4/2
2	2/3	6/2/2	7/8/4/6
3	2/4	6/2/3	7/8/4/8
4	2/7	6/2/4	7/8/4/10
5	2/14	6/2/6	7/8/4/12

stoichiometric ratio of Al/Si/Ca is provided in SI Tables S1. A planetary ball-mill apparatus (QM-3SP2, Nanjing Nanda, China) was used for the homogeneous mixing of samples. Total 20 g of the weighted sample was put into a agate pot of 100 mL inner volume with 15 agate balls of 30 mm in diameter, and the mill was run for 240 min (20 min grinding and 10 min pause in turn) under ambient atmosphere at rotational speeds of 300 rpm. 5 g of derived mixture was then pressed into one pellet with a diameter of 30 mm and a thickness of ~5 mm. To ensure consistent compaction of the powder sample, the pressure was all held at 20 MPa for 1 min by Electric tablet press (YLJ-30TA, Shenyang Kejing, China). The pellets were then transferred into a high temperature muffle furnace (SX-G13163, Tianjin Zhonghuan, China) and sintered at targeted temperatures with increasing rates of 5 °C/min for 2 h, and then quenched in air to room temperature. Mullite was reported as the only stable binary crystalline phase in the SiO<sub>2</sub>–Al<sub>2</sub>O<sub>3</sub> system, and the effect of temperature on crystal growth of mullite was exhaustively studied [19, 21, 24–26]. Thus, samples in Al<sub>2</sub>O<sub>3</sub>/tailing and Al<sub>2</sub>O<sub>3</sub>/SiO<sub>2</sub>/tailing systems were studied as a function of mass ratio of Al<sub>2</sub>O<sub>3</sub>/tailing and Al<sub>2</sub>O<sub>3</sub>/SiO<sub>2</sub>/tailing, and sintered at 1450 °C for 2 h. Samples in Al<sub>2</sub>O<sub>3</sub>/SiO<sub>2</sub>/CaO/tailing system were examined as functions of mass ratios of Al<sub>2</sub>O<sub>3</sub>/SiO<sub>2</sub>/CaO/tailing and temperature, and were sintered at temperatures of 950 °C to 1450 °C for 2 h. Triplicate samples were set for each group, and the results were averaged.

### X-ray Diffraction (XRD) and Scanning Electron Microscopy (SEM) Analysis

The sintered samples were ground into powder with a particle size of less than 200 µm for XRD analysis. The powder XRD patterns were recorded on a Bruker D8 Advance X-ray powder diffractometer. The crystalline phases of the obtained XRD patterns were analyzed by matching with standard database through Eva XRD Pattern Processing software (Bruker Co. Ltd.). The crystalline phases found in the products included mullite (3Al<sub>2</sub>O<sub>3</sub>·2SiO<sub>2</sub>, PDF #79-1276), anorthite (CaAl<sub>2</sub>Si<sub>2</sub>O<sub>8</sub>, PDF #89-1471), gehlenite (Ca<sub>2</sub>Al<sub>2</sub>SiO<sub>7</sub>, PDF #77-1146), cristobalite (SiO<sub>2</sub>, PDF #77-1316), quartz (SiO<sub>2</sub>, PDF #85-0335), lime (CaO, PDF #99-0070), corundum (α-Al<sub>2</sub>O<sub>3</sub>, PDF#74-1081), hematite (Fe<sub>2</sub>O<sub>3</sub>, PDF #99-0060), and magnetite (Fe<sub>3</sub>O<sub>4</sub>, PDF #87-2334).

With the addition of 15 wt% CaF<sub>2</sub> (0.15 g CaF<sub>2</sub> mixed with 0.85 g sample) as the internal standard [27–29], quantitative refinement method was used to quantify the content of both amorphous and crystalline phases in the samples. XRD scans were conducted from 2θ = 10° to 110°, with a step width of 2θ = 0.02° and a sampling time of 0.5 s per step. The Rietveld refinements for phase quantification were processed by the TOPAS (version 4.0) program. Structure

models of the crystalline phases were obtained from the ICDD database. Figures S2–S6 present the Rietveld refinement plots of the glass ceramics sintered from the systems of tailing, Al<sub>2</sub>O<sub>3</sub>/tailing, Al<sub>2</sub>O<sub>3</sub>/SiO<sub>2</sub>/tailing, and Al<sub>2</sub>O<sub>3</sub>/SiO<sub>2</sub>/CaO/tailing, and the corresponding reliability values, indicating the good refinement quality achieved using this analytical scheme, are provided in SI Tables S2–S6.

The microstructure of produced samples was observed by a field emission scanning electron microscope (FESEM, SU8220, Hitachi, Japan). The surfaces of the obtained glass ceramics were polished by the metallographic grinding and polishing machine (Metaserv250, Buehler), and the polished samples were coated with gold for SEM analysis.

### Measurements of Mechanical Properties, Chemical Resistance, and Water Adsorption

The compressive strength of products was investigated by using a universal material testing machine (INSTRON 5967, USA) at a cross-head speed of 1 mm/min [15]. The chemical resistances evaluation was estimated according to the JC/T 872-2000 building material industry standard. The products were immersed in 1% H<sub>2</sub>SO<sub>4</sub> and 1% NaOH solutions for 650 h, the liquid level was 30 mm higher than the samples. For each test, at least five samples were tested and the results were averaged. The acid/alkali resistance (K) of the glass ceramic was calculated by Eq. (1):

$$K = (m_1 - m_2) / m_1 \times 100\% \quad (1)$$

where  $m_1$  is the mass of samples before corrosion and  $m_2$  is the mass of samples after corrosion. The water adsorption (%) of samples was determined according to Chinese Standard (GB/T 9966.3-2001). The samples were dried at 105 °C to a constant weight, then the dried samples were soaked in distilled water at 20 °C for 48 h. The moisture on the surface was wiped off with a wrung towel after taking out them.

### Toxicity Characteristic Leaching

To assess the stabilization of glass ceramic materials, samples were subjected to toxicity characteristic leaching procedure modified from the U.S. EPA SW-846 Method 1311 TCLP with a pH 4.9 acetic acid solution (extraction fluid # 1) as the leaching fluid [30, 31]. The leaching solution used in the experiment consists of 5.7 mL of acetic acid diluted in 500 mL of deionized water, in which 64.3 mL of 1 M NaOH was added and the resulting solution was diluted with deionized water to the volume of 1 L. The pH of the solution was finally maintained at 4.93 ± 0.05. Each leaching vial solution contained 10 mL of extraction fluid and 0.5 g of powder (L/S = 20). The leaching vial was rotated end-over-end at 100 rpm for 120 days. At the end of each agitation period,

the leachates were filtered using 0.45  $\mu\text{m}$  filters and heavy metals were determined by inductively coupled plasma optical emission spectroscopy (ICP-OES) using a Perkin-Elmer Optima DV2100 instrument.

## Results and Discussion

### Effect of Temperature Effect on Tailing-Based Glass Ceramics

As sintering temperature plays an important role for glass ceramic production [19, 21, 22, 25], the samples of iron tailing and  $\text{Al}_2\text{O}_3/\text{SiO}_2/\text{CaO}/\text{tailing}$  were sintered at a wide temperature range of 950–1450  $^\circ\text{C}$  (Fig. 1), for observing the crystal transformation. XRD patterns for sintering iron tailing at temperatures of 950–1450  $^\circ\text{C}$  are demonstrated in Fig. 1a. It can be found that the main crystalline phases in raw tailing are goethite ( $\text{FeOOH}$ ) and quartz ( $\text{SiO}_2$ ). With the increase of temperatures from 950 to 1350  $^\circ\text{C}$ , the disappearance of goethite and significant formation of hematite ( $\text{Fe}_2\text{O}_3$ ) were observed, indicating the crystal transformation of goethite into hematite. In addition, the decrease of peak intensity of quartz ( $\text{SiO}_2$ ) and increase of cristobalite ( $\text{SiO}_2$ ) suggested that quartz transformed into cristobalite at higher temperatures of 1180–1350  $^\circ\text{C}$ . At 1450  $^\circ\text{C}$ , the transformation of hematite into magnetite ( $\text{Fe}_3\text{O}_4$ ) was observed. Figure 1a suggests that sintering iron tailing alone prompted the transformation of raw materials of goethite and quartz into hematite and cristobalite, respectively, but no reaction between the raw materials was detected.

Comparing with sintering iron tailing alone, four crystalline phases, quartz, cristobalite, lime ( $\text{CaO}$ ), and hematite, could be identified as initial minerals at 950  $^\circ\text{C}$  for sample of  $\text{Al}_2\text{O}_3/\text{SiO}_2/\text{CaO}/\text{tailing}$  mass ratio of 7/8/4/6 (Fig. 1b). At 1100  $^\circ\text{C}$ , the diffraction peak of lime disappeared, along with the appearance of a small amount of gehlenite ( $\text{Ca}_2\text{Al}_2\text{SiO}_7$ ). The formation of  $\text{Ca}_2\text{Al}_2\text{SiO}_7$  during the sintering process was probably initiated by the reaction among  $\text{CaO}$ ,  $\text{Al}_2\text{O}_3$ , and  $\text{SiO}_2$ . At 1180  $^\circ\text{C}$ , the formation of crystalline anorthite ( $\text{CaAl}_2\text{Si}_2\text{O}_8$ ) [32] was observed. When the temperature increased from 1200 to 1250  $^\circ\text{C}$ , the decrease of peak intensity in gehlenite and the growth of anorthite were detected. Such findings suggested an intermediate compound (i.e., gehlenite,  $\text{Ca}_2\text{Al}_2\text{SiO}_7$ ) appeared at 1180–1250  $^\circ\text{C}$ . As solid-state reaction is generally influenced by the encounter rate between reactant molecules [33], the low temperature (1180–1250  $^\circ\text{C}$ ) did not allow sufficient contact of  $\text{SiO}_2$ ,  $\text{Al}_2\text{O}_3$ , and  $\text{CaO}$  molecules, resulting in the formation of intermediate phase, gehlenite. With the increase of temperature (> 1250  $^\circ\text{C}$ ), the peak intensity of intermediate gehlenite disappeared, while anorthite was detected as the mainly crystalline phase in the system. When temperatures

increased from 1300 to 1450  $^\circ\text{C}$ , reactants would have more intensive interactions, and the significant increase of anorthite was observed.

In addition, the Bragg reflection of initial materials (i.e., hematite, lime, cristobalite, and quartz) was decreased by increasing temperatures from 950 to 1450  $^\circ\text{C}$ . Lime, cristobalite, and quartz would react with  $\text{Al}_2\text{O}_3$  for the crystallization of anorthite. However, no newly formed Fe-containing crystalline phase was observed, the results indicated that hematite may react with lime, quartz, and aluminosilicate to form eutectics with amorphous structures at high temperature of 1450  $^\circ\text{C}$  [34, 35].

To determine the content of crystalline and amorphous phases in sintered tailing and  $\text{Al}_2\text{O}_3/\text{SiO}_2/\text{CaO}/\text{tailing}$  glass ceramics, quantitative XRD analysis was performed by Rietveld and internal standard method. The phase contents of crystalline and amorphous phase(s) of sintered tailing and  $\text{Al}_2\text{O}_3/\text{SiO}_2/\text{CaO}/\text{tailing}$  glass ceramics are demonstrated in Fig. 1c and d. Figure 1c presents the contents of crystalline and amorphous phase(s) in tailing samples sintered at 950–1450  $^\circ\text{C}$  for 2 h. The compositions of hematite firstly increased, and reached its maximum (32.1 wt%) at 1200  $^\circ\text{C}$ , and then decreased with the increased temperature. At 1450  $^\circ\text{C}$ , the transformation of hematite into magnetite was observed, and the content of magnetite increased to 9.0 wt%. The content of quartz firstly increased to 6.8 wt% and then decreased, because of its transformation into cristobalite at 1350–1450  $^\circ\text{C}$ . The content of amorphous phase(s) maintained at 60–86 wt% in sintered iron tailing, which indicated that  $\text{Al}_2\text{O}_3$  and most of  $\text{SiO}_2$  in iron tailing may exist in amorphous phase(s). Figure 1d summarizes the weight fractions of crystalline and amorphous phase(s) in sample with  $\text{Al}_2\text{O}_3/\text{SiO}_2/\text{CaO}/\text{tailing}$  mass ratio of 7/8/4/6 sintered at 950–1450  $^\circ\text{C}$  for 2 h. Three stages of phase transformation were observed, representing different crystallization behaviors at temperature range of 950–1450  $^\circ\text{C}$ . In the first stage (950–1100  $^\circ\text{C}$ ), almost no reaction between the raw materials was detected, the compositions of hematite, cristobalite, and corundum maintained at ~6, ~12, and ~5 wt%. The initial formation of gehlenite (~7.7 wt%), as an intermediate phase, was observed at this stage. At second stage (1180–1300  $^\circ\text{C}$ ), hematite, cristobalite, corundum, and intermediate gehlenite disappeared, and the significant crystallization of anorthite (from 4.1 to 65 wt%) was detected, indicating intensive interaction between reactants of  $\text{CaO}$  with  $\text{SiO}_2$  and  $\text{Al}_2\text{O}_3$ . Correspondingly, the content of the amorphous phase showed a downward trend from 66.1 to 34.9 wt%, may be caused by the entrance of amorphous  $\text{Al}_2\text{O}_3$  and  $\text{SiO}_2$  into the crystalline anorthite structure [36]. In the third stage (1350–1450  $^\circ\text{C}$ ), anorthite was found to be the only crystalline phase in the sample. The content of anorthite maintained at 65.1–67.8

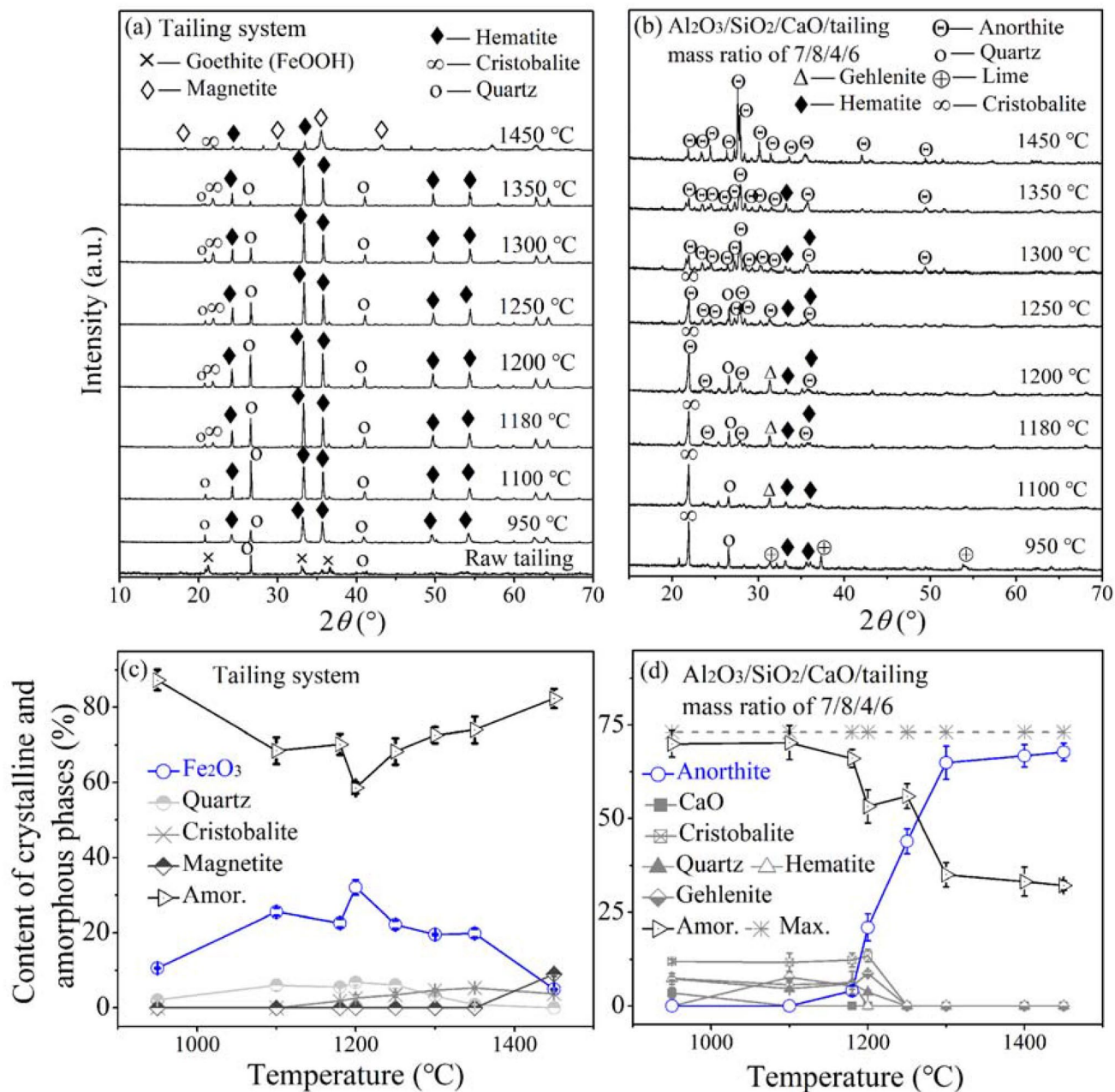


**Fig. 1** XRD spectra of glass ceramic samples in **a** tailing system; **b** sample of  $\text{Al}_2\text{O}_3/\text{SiO}_2/\text{CaO}/\text{tailing}$  mass ratio of 7/8/4/6 sintered at 950–1450 °C for 2 h; Content of crystalline and amorphous phases quantified by QXRD in **c** tailing system and **d** sample of  $\text{Al}_2\text{O}_3/\text{SiO}_2/\text{CaO}/\text{tailing}$  mass ratio of 7/8/4/6 sintered at 950–1450 °C for

2 h. The solid line of amor. is the calculated content of amorphous phase(s) in glass ceramics. The dashed line of max. is the maximum predicted contents for the formation of anorthite based on the initial content of  $\text{SiO}_2$ ,  $\text{Al}_2\text{O}_3$ , and CaO in glass ceramics

wt% at this stage, suggesting a high transformation ratio (~92.8 wt%) of incorporating tailing,  $\text{Al}_2\text{O}_3$ ,  $\text{SiO}_2$ , and CaO into anorthite phase. By comparing with sintering tailing alone, the addition of CaO significantly promoted the formation of anorthite at 1450 °C, which was considered as the optimal temperature for sintering tailing-based glass ceramics.

### Effect of $\text{Al}_2\text{O}_3$ , $\text{SiO}_2$ , and CaO Addition on Tailing-Based Glass Ceramics

To investigate the effect of  $\text{Al}_2\text{O}_3$ ,  $\text{SiO}_2$ , and CaO addition on crystallization behavior of glass ceramics, products in  $\text{Al}_2\text{O}_3/\text{tailing}$ ,  $\text{Al}_2\text{O}_3/\text{SiO}_2/\text{tailing}$ , and  $\text{Al}_2\text{O}_3/\text{SiO}_2/\text{CaO}/\text{tailing}$  systems sintered at 1450 °C for 2 h were analyzed by

XRD (Fig. 2). As shown in Fig. 2a and b, the newly formed crystalline phase, mullite ( $3\text{Al}_2\text{O}_3 \cdot 2\text{SiO}_2$ ), was observed in  $\text{Al}_2\text{O}_3/\text{tailing}$  and  $\text{Al}_2\text{O}_3/\text{SiO}_2/\text{tailing}$  systems. The formation of mullite was initiated by the reaction of  $\text{Al}_2\text{O}_3$  with  $\text{SiO}_2$  [19, 21, 24–26]. However, the main crystalline phase was found to be anorthite ( $\text{CaAl}_2\text{Si}_2\text{O}_8$ ) in  $\text{Al}_2\text{O}_3/\text{SiO}_2/\text{CaO}/\text{tailing}$  system, due to the reaction of  $\text{CaO}$  with  $\text{Al}_2\text{O}_3$  and  $\text{SiO}_2$  [32].

The crystal growth of mullite was firstly increased, and reached its maximum at mass ratio of  $\text{Al}_2\text{O}_3/\text{tailing}$  of 2/3 (Al/Si molar ratio of 6/2). With further addition of tailing, peak intensity of mullite decreased, as shown in Fig. 2a. Similarly, the intensity of mullite firstly increased with the addition of tailing and reached its highest value at mass ratio of  $\text{Al}_2\text{O}_3/\text{SiO}_2/\text{tailing}$  of 6/2/2 (Al/Si molar ratio of 6/2) in  $\text{Al}_2\text{O}_3/\text{SiO}_2/\text{tailing}$  system. The reduction of mullite intensity was detected with further addition of tailing by decreasing  $\text{Al}_2\text{O}_3/\text{SiO}_2/\text{tailing}$  mass ratio from 6/2/2 to 6/2/6 (Fig. 2b). The above results suggested that crystal growth of mullite can be significantly improved at Al/Si molar ratio of 6/2 in both  $\text{Al}_2\text{O}_3/\text{tailing}$  and  $\text{Al}_2\text{O}_3/\text{SiO}_2/\text{tailing}$  systems, which is

also the stoichiometric ratio of Al/Si in mullite compound. In addition, the minor phase of hematite showed a slight increase with the addition of tailing in systems of  $\text{Al}_2\text{O}_3/\text{tailing}$  and  $\text{Al}_2\text{O}_3/\text{SiO}_2/\text{tailing}$ . In contrast, minor phases of cristobalite and corundum decreased with the addition of tailing because of the incorporation of  $\text{Al}_2\text{O}_3$  and  $\text{SiO}_2$  into mullite.

Figure 2c displays XRD spectrums of samples in  $\text{Al}_2\text{O}_3/\text{SiO}_2/\text{CaO}/\text{tailing}$  system sintered at  $1450^\circ\text{C}$  for 2 h. The main crystalline phase was found to be anorthite ( $\text{CaAl}_2\text{Si}_2\text{O}_8$ ). The peak intensity of anorthite firstly increased, and then decreased with the addition of tailing in  $\text{Al}_2\text{O}_3/\text{SiO}_2/\text{CaO}/\text{tailing}$  system. Sample with  $\text{Al}_2\text{O}_3/\text{SiO}_2/\text{CaO}/\text{tailing}$  mass ratio of 7/8/4/6 (Al/Si/Ca molar ratio of 2/2/1) was detected as the favorable composition for anorthite crystallization. In addition, except hematite and magnetite, no newly formed Fe-containing crystalline phase was observed at samples with high content of iron tailing. The results indicated that hematite can transform into magnetite and also may react with lime, quartz, and aluminosilicate to form amorphous structures at  $1450^\circ\text{C}$  [34, 35].

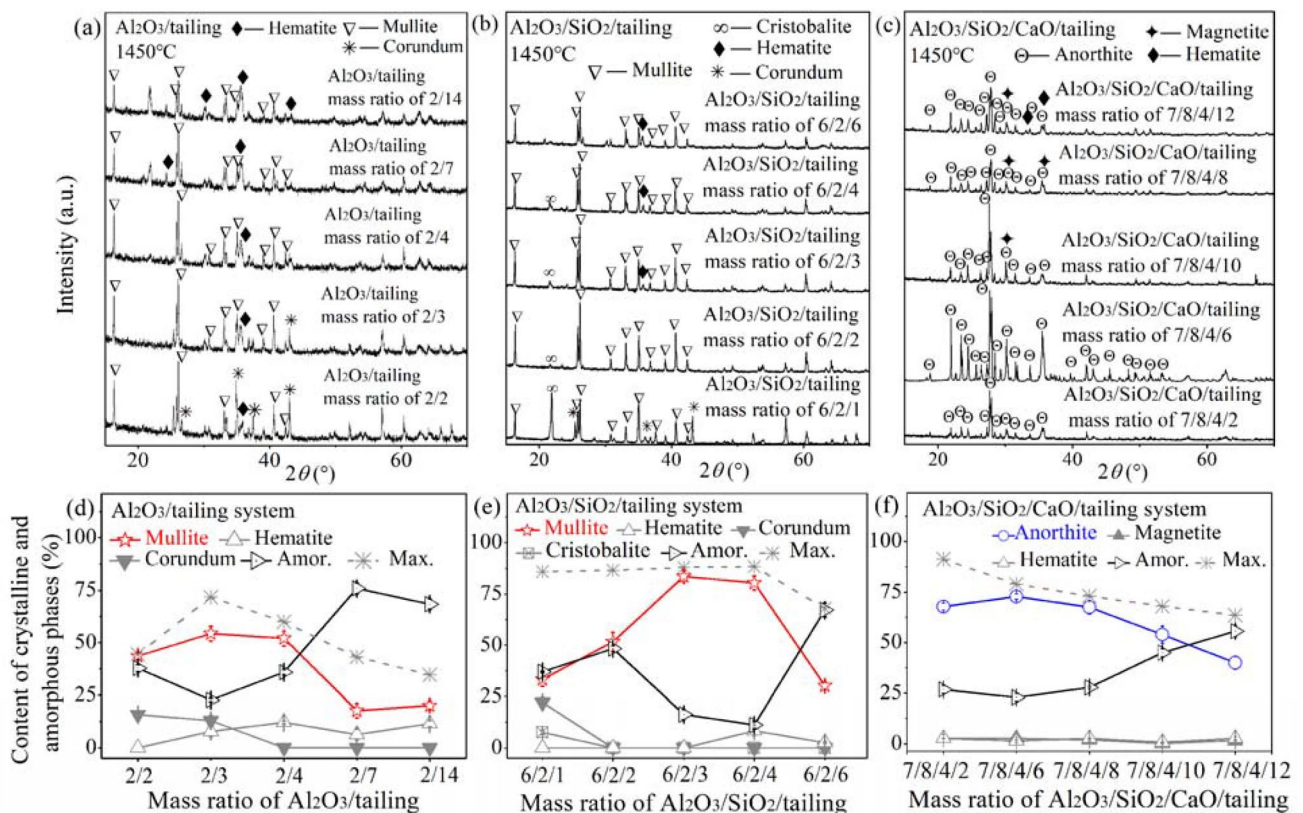


**Fig. 2** The XRD spectrums of glass ceramic samples in **a**  $\text{Al}_2\text{O}_3/\text{tailing}$  system; **b**  $\text{Al}_2\text{O}_3/\text{SiO}_2/\text{tailing}$  system; **c**  $\text{Al}_2\text{O}_3/\text{SiO}_2/\text{CaO}/\text{tailing}$  system sintered at  $1450^\circ\text{C}$  for 2 h; content of crystalline and amorphous phases quantified by QXRD in **d**  $\text{Al}_2\text{O}_3/\text{tailing}$  system; **e**  $\text{Al}_2\text{O}_3/\text{SiO}_2/\text{tailing}$  system; **f**  $\text{Al}_2\text{O}_3/\text{SiO}_2/\text{CaO}/\text{tailing}$  system sintered

at  $1450^\circ\text{C}$  for 2 h. The solid line of amor. is the calculated content of amorphous phase(s) in glass ceramics. The dashed line of max. is the maximum predicted contents for the formation of mullite and anorthite based on the initial content of  $\text{SiO}_2$ ,  $\text{Al}_2\text{O}_3$ , and  $\text{CaO}$  in glass ceramics

The phase contents of crystalline and amorphous phase(s) in  $\text{Al}_2\text{O}_3$ /tailing,  $\text{Al}_2\text{O}_3$ / $\text{SiO}_2$ /tailing, and  $\text{Al}_2\text{O}_3$ / $\text{SiO}_2$ /CaO/tailing systems are demonstrated in Fig. 2. In  $\text{Al}_2\text{O}_3$ /tailing system (Fig. 2d), the content of mullite firstly increased, followed by the decrease of contents of cristobalite and corundum with the addition of tailing, as  $\text{Al}_2\text{O}_3$  reacted with  $\text{SiO}_2$  for the formation of mullite. The content of mullite reached its maximum of 54.3 wt% at  $\text{Al}_2\text{O}_3$ /tailing mass ratio of 2/3. When  $\text{Al}_2\text{O}_3$ /tailing mass ratio decreased from 2/3 to 2/14, the gradual decrease of mullite followed by the increase of amorphous and hematite phases were detected. The slight increase of hematite content is due to the addition of tailing into  $\text{Al}_2\text{O}_3$ /tailing systems. The significant increase of amorphous phase(s) (from 22.7 to 68.4 wt%) would be caused by the potential reaction of hematite with aluminosilicate for the formation of amorphous structures in the products [34, 35, 37]. The content of crystalline and amorphous phases in  $\text{Al}_2\text{O}_3$ / $\text{SiO}_2$ /tailing system is shown in Fig. 2e. The highest mullite content (~83.7 wt%) was detected at  $\text{Al}_2\text{O}_3$ / $\text{SiO}_2$ /tailing mass ratio of 6/2/2, which represent a nearly 95.0% transformation of  $\text{Al}_2\text{O}_3$  and  $\text{SiO}_2$  into mullite phase. Correspondingly, the content of corundum and cristobalite decreased gradually due to the substantial crystallization of mullite. When  $\text{Al}_2\text{O}_3$ / $\text{SiO}_2$ /tailing mass ratio changed from 6/2/2 to 6/2/6, the content of mullite reduced from 83.7 to 30.2 wt%, whereas the content of amorphous phase(s) increased from 16.3 to 67.2 wt%. This finding demonstrated the partial amorphization in  $\text{Al}_2\text{O}_3$ / $\text{SiO}_2$ /tailing system with the further addition of iron tailing, and suggested the potential reaction of hematite with aluminosilicate to form glass phase(s) [34, 35, 37]. Furthermore, the formation of amorphous phase(s) was reported to inhibit the growth of the crystal, because it increases the viscosity of the glass and makes crystallization difficult [38].

Figure 2f shows that the maximum content of anorthite (~72.9 wt%) was found for sample with  $\text{Al}_2\text{O}_3$ / $\text{SiO}_2$ /CaO/tailing mass ratio of 7/8/4/6, which represented a nearly ~92.3% transformation of  $\text{Al}_2\text{O}_3$ ,  $\text{SiO}_2$ , and CaO into the anorthite phase. The results indicated a substantial crystallization of  $\text{SiO}_2$  with  $\text{Al}_2\text{O}_3$  and CaO for the formation of anorthite in  $\text{Al}_2\text{O}_3$ / $\text{SiO}_2$ /CaO/tailing system. With the addition of tailing, the phase content of hematite and magnetite maintained at 1~2 wt%. However, the composition of amorphous phase(s) increased from 26.7 to 55.7 wt%. The results indicated that hematite would react with aluminosilicate to form amorphous phases [34, 35].

### SEM Analysis for Tailing-Based Glass Ceramic

SEM micrographs of samples in  $\text{Al}_2\text{O}_3$ /tailing,  $\text{Al}_2\text{O}_3$ / $\text{SiO}_2$ /tailing, and  $\text{Al}_2\text{O}_3$ / $\text{SiO}_2$ /CaO/tailing systems are summarized in Fig. 3. As shown in Fig. 3a–c, the samples in  $\text{Al}_2\text{O}_3$ /tailing system displayed lots of pores on

surface with different sizes. The pores in samples with  $\text{Al}_2\text{O}_3$ /tailing mass ratio of 2/2 to 2/4 are spherical with average diameter of 50–100  $\mu\text{m}$ . With the further addition of iron tailing, the intensive reaction of hematite with aluminosilicate may lead to the formation of glass phase, which impeded the escape of gas and reduced the pore size Lu et al. [28] and the mean diameter of pores reduced to 3–5  $\mu\text{m}$ , as shown in Fig. 3d and e.

In  $\text{Al}_2\text{O}_3$ / $\text{SiO}_2$ /tailing system, sample with  $\text{Al}_2\text{O}_3$ / $\text{SiO}_2$ /tailing mass ratio of 6/2/1 (Fig. 3f) was found with isolated grain particles on the surface. With the addition of tailing, the porous surface of samples with pore diameter of 50–100  $\mu\text{m}$  is observed in Fig. 3h and i, indicating the densification between tailing and precursors. However, these pores turn to be closed structure and slight glassy surface was detected with the further addition of tailing in sample with  $\text{Al}_2\text{O}_3$ / $\text{SiO}_2$ /tailing mass ratio of 6/2/2 (Fig. 3j). The overall results may indicate that hematite from tailing was partially reacted with quartz and aluminosilicate within combustion process [34, 35, 39], leading to the formation of eutectics with dense surface structures in  $\text{Al}_2\text{O}_3$ / $\text{SiO}_2$ /tailing system.

Figure 3k–o exhibits different surface microstructures of glass ceramic samples in  $\text{Al}_2\text{O}_3$ / $\text{SiO}_2$ /CaO/tailing system. The surface of the sample with mass ratio of  $\text{Al}_2\text{O}_3$ / $\text{SiO}_2$ /CaO/tailing of 7/8/4/2 (Fig. 3k) is pitted with subsidence holes. With the addition of tailing, a condensed surface of sample with  $\text{Al}_2\text{O}_3$ / $\text{SiO}_2$ /CaO/tailing mass ratio of 7/8/4/6 was observed (Fig. 3l). Compared to Fig. 3k and l, the glass ceramics with high iron tailing content (Fig. 3m–o) have the relatively smooth surfaces. The results suggested the interaction between hematite and lime, quartz and aluminosilicate to form a dense surface structure at sintered process [34, 35]. Figure 3p–t illustrates the SEM images of sintered glass ceramics with  $\text{Al}_2\text{O}_3$ / $\text{SiO}_2$ /CaO/tailing mass ratio of 7/8/4/6 at different temperatures of 1250–1450 °C. At lower temperatures of 1250–1300 °C (Fig. 3p and q), the samples show porous surfaces with pore diameter of 25–100  $\mu\text{m}$ , which were formed due to the escape of gases during the sintering process [28]. With the increase of temperature to 1350 °C, the porosity of glass ceramics was greatly reduced. When the temperature further increased to 1400–1450 °C, the superficial pores disappeared and sample showed dense surface structure.

### Properties of Tailing-Based Glass Ceramics

Figure 4a summarizes that the compressive strength firstly increased and decreased with the addition of tailing in  $\text{Al}_2\text{O}_3$ /tailing system. As compressive strength was directly related to the content of crystalline phase(s) in samples [28], the compressive strength increased as the increase of mullite

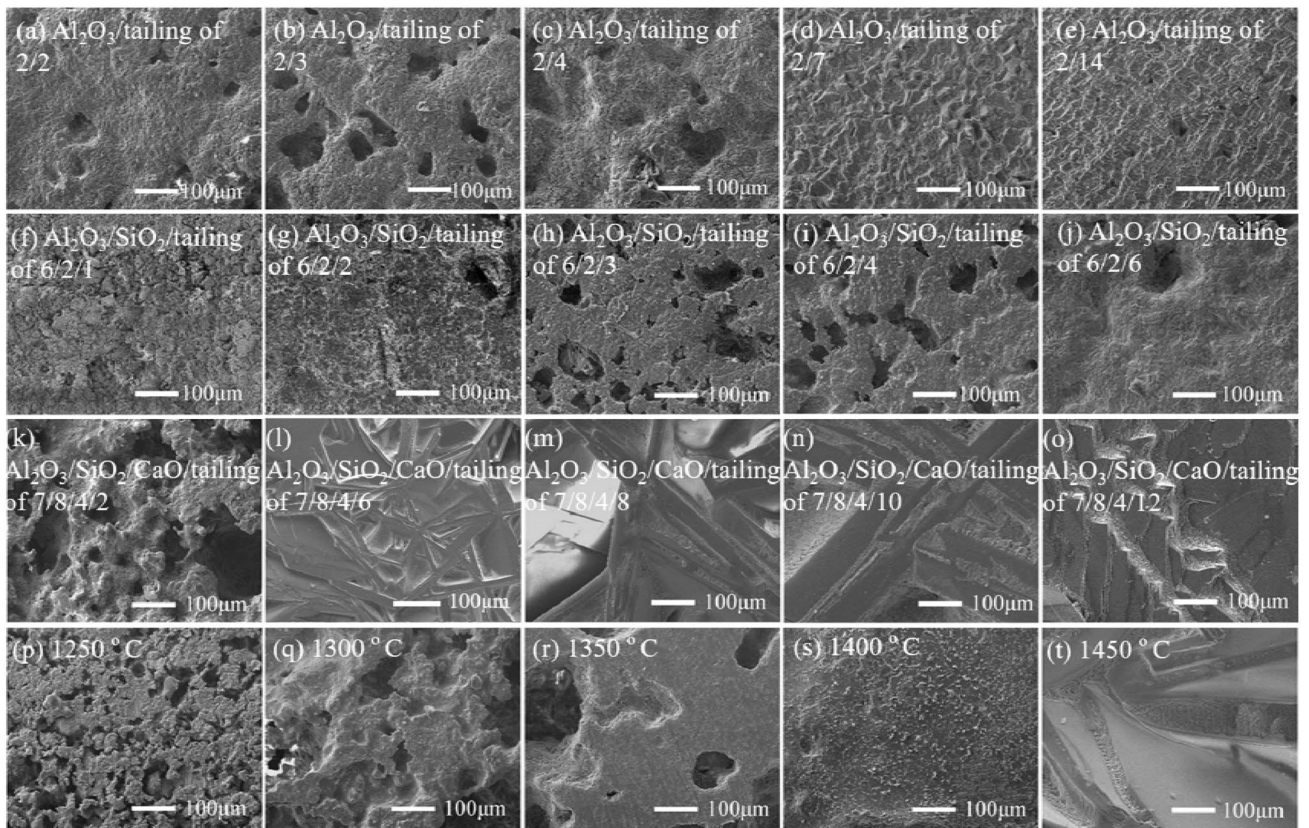


**Fig. 3** SEM micrographs of glass ceramic samples in (a–e)  $\text{Al}_2\text{O}_3$ /tailing system; (f–j)  $\text{Al}_2\text{O}_3/\text{SiO}_2$ /tailing system; (k–o)  $\text{Al}_2\text{O}_3/\text{SiO}_2/\text{CaO}$ /tailing system sintered at 1450 °C for 2 h; and (p–t) sample of  $\text{Al}_2\text{O}_3/\text{SiO}_2/\text{CaO}$ /tailing mass ratio of 7/8/4/6 sintered at 1250–1450 °C for 2 h

content in  $\text{Al}_2\text{O}_3$ /tailing system. The sample of  $\text{Al}_2\text{O}_3$ /tailing mass ratio of 2/3 with the highest mullite content had the maximum compressive strength of 968.6 MPa. However, the compressive strength decreased to 395.6 MPa, as mullite content decreased substantially with the further increase of tailing content ( $\text{Al}_2\text{O}_3$ /tailing mass ratio decreased from 2/3 to 2/14). Figure 4b suggests that with samples of  $\text{Al}_2\text{O}_3/\text{SiO}_2$ /tailing mass ratios changed from 6/2/1 to 6/2/2, their compressive strength increased from 450.6 to 925.5 Mpa, due to the increase of mullite content in glass ceramics. However, the compressive strength of the sample shows a slight increase from 907.6 to 1061.2 Mpa, with the decrease of mullite content in samples with  $\text{Al}_2\text{O}_3/\text{SiO}_2$ /tailing mass ratios changed from 6/2/3 to 6/2/6. The results may indicate that the network structure of  $\text{Al}_2\text{O}_3/\text{SiO}_2$ /tailing system was enhanced by the condensed surface structure, caused by the formation of eutectics with amorphous structures by reaction of hematite with aluminumsilicate [34, 35, 40]. Figure 4c exhibits the compressive strength of sintered glass ceramics with different tailing contents in  $\text{Al}_2\text{O}_3/\text{SiO}_2/\text{CaO}$ /tailing system. The maximum value of compressive strength was observed to be 905.35 MPa in the sample with  $\text{Al}_2\text{O}_3/\text{SiO}_2/\text{CaO}$ /tailing mass ratio of 7/8/4/6, which had the highest

content of anorthite and lowest surface porosity. Figure 4d indicates that the compressive strength increased from 203.6 to 733.61 Mpa, due to the crystal growth of anorthite with temperature increased from 1250 to 1450 °C [41].

Figure 5a shows that the water absorption ratio was firstly increased and then decreased in  $\text{Al}_2\text{O}_3$ /tailing system. The lowest water absorption ratio (0.4%) was observed for sample with  $\text{Al}_2\text{O}_3$ /tailing mass ratio of 2/14, which was with the most compact surface structure. In  $\text{Al}_2\text{O}_3/\text{SiO}_2$ /tailing system (Fig. 5b), the water absorption ratio decreased from 31.4 to 0.2% when mass ratios of  $\text{Al}_2\text{O}_3/\text{SiO}_2$ /tailing changed from 6/2/1 to 6/2/2, due to the reduced surface porosity of the samples [11, 42, 43]. In  $\text{Al}_2\text{O}_3/\text{SiO}_2/\text{CaO}$ /tailing system (Fig. 5c), the water absorption ratio decreased from 25.4 to 0.31% when mass ratio of  $\text{Al}_2\text{O}_3/\text{SiO}_2/\text{CaO}$ /tailing changed from 7/8/4/2 to 7/8/4/6, and maintained at 0.3–0.5% with mass ratio of  $\text{Al}_2\text{O}_3/\text{SiO}_2/\text{CaO}$ /tailing changed from 7/8/4/8 to 7/8/4/12. Similarly, the water absorption ratio decreased with the reduced surface porosity of samples in  $\text{Al}_2\text{O}_3/\text{SiO}_2/\text{CaO}$ /tailing system.

As demonstrated in Fig. 5d, the water absorption ratio decreased with the increase of sintering temperature from 1250 to 1450 °C in sample with  $\text{Al}_2\text{O}_3/\text{SiO}_2/\text{CaO}$ /tailing

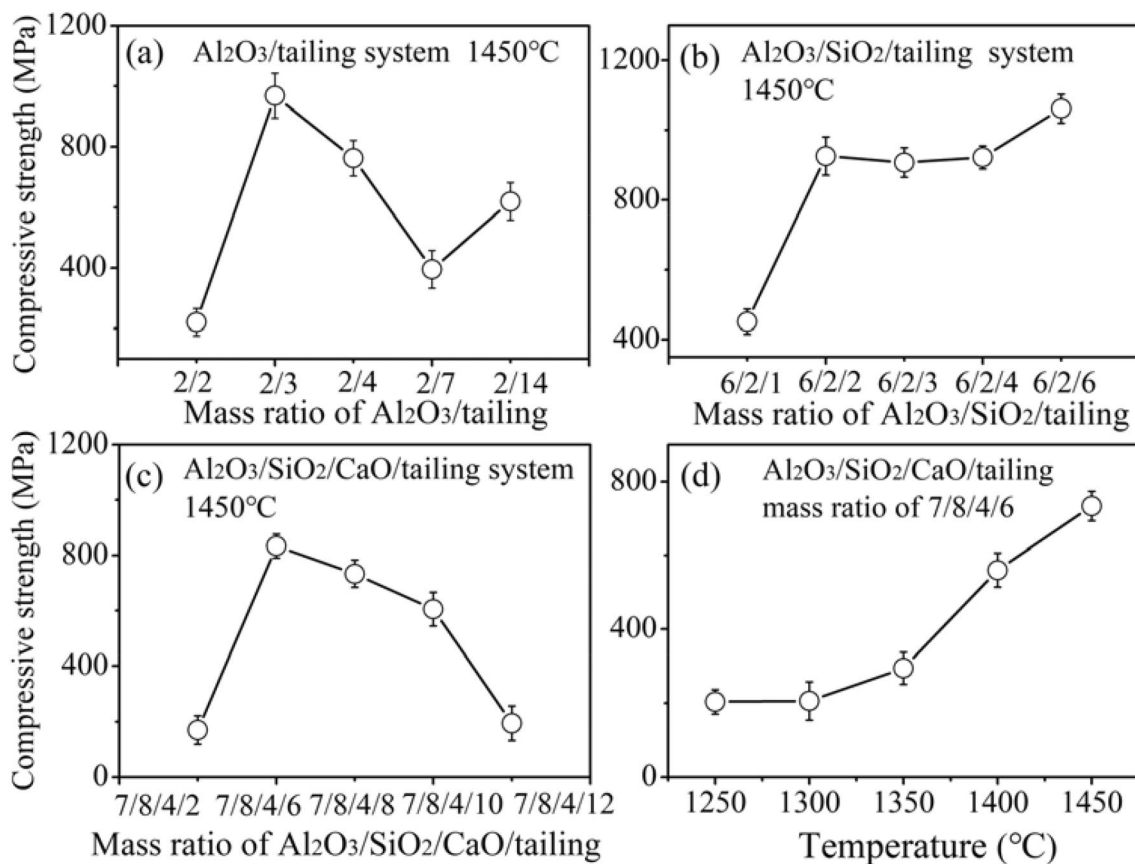


**Fig. 4** The compressive strength of glass ceramics in **a** Al<sub>2</sub>O<sub>3</sub>/tailing system; **b** Al<sub>2</sub>O<sub>3</sub>/SiO<sub>2</sub>/tailing system; **c** Al<sub>2</sub>O<sub>3</sub>/SiO<sub>2</sub>/CaO/tailing system sintered at 1450 °C for 2 h; and **d** sample of Al<sub>2</sub>O<sub>3</sub>/SiO<sub>2</sub>/CaO/tailing mass ratio of 7/8/4/6 sintered at 1250–1450 °C for 2 h

mass ratio of 7/8/4/6. Such results also suggested that the water absorption ratio decreased with the reduced porosity of the microstructure due to temperature increase. Overall, it can be concluded that the increase of tailing content and temperature would form amorphous phase with dense surface structure, thereby decreasing the water absorption ratio of glass ceramic samples.

In samples of Al<sub>2</sub>O<sub>3</sub>/tailing, Al<sub>2</sub>O<sub>3</sub>/SiO<sub>2</sub>/tailing, and Al<sub>2</sub>O<sub>3</sub>/SiO<sub>2</sub>/CaO/tailing systems, Fig. 6a–c shows that both acid and alkali resistance increased with the addition of iron tailings content. The increased content of iron tailing promoted the interaction between hematite and aluminumsilicate to form glass phases with dense surface structure [34, 35, 39], as a result, increased the acid and alkali resistance of glass ceramics. Figure 6d demonstrates that the chemical durability of sample with Al<sub>2</sub>O<sub>3</sub>/SiO<sub>2</sub>/CaO/tailing mass ratio of 7/8/4/6 significantly increased with the increase of sintering temperature from 1250 to 1450 °C. The improvement in chemical durability can also be attributed to the reduced porosity of the micro surface. Additionally, obtained glass ceramic mainly had better resistance when soaked in alkaline solution (NaOH) than in acidic solution (H<sub>2</sub>SO<sub>4</sub>),

as shown in Fig. 6. The main reason would be the presence of high amount of alkali components (e.g., SiO<sub>2</sub> and CaO) in glass ceramics, which can resist the abrasion of alkaline solution [44, 45]

Overall, the obtained glass ceramics were determined with excellent chemical resistance of 79.3–99.99%, water absorption ratio of 0.2–31.3%, and compressive strength values of 170.3–1061.6 MPa, and the results are superior or compatible to those of common commercial materials (chemical resistance of 70–99%, water absorption ratio of 0.02–0.05%, and compressive strength of 900–1200 MPa), as reported in the literatures [46–48]. Leaching test results of hazardous Pb, Zn, Cu, Cr, and Ni from raw tailings, heated raw tailings, and glass ceramic with Al<sub>2</sub>O<sub>3</sub>/SiO<sub>2</sub>/CaO/tailing mass ratio of 7/8/4/6 sintered at 1450 °C are shown in Table S7. Concentrations of Pb, Zn, and Cu in leachate of Al<sub>2</sub>O<sub>3</sub>/SiO<sub>2</sub>/CaO/tailing mass ratio of 7/8/4/6 sintered at 1450 °C were 0.09, 0.26, 1.74 mg/L and Cr and Ni were below the detection limit. The results indicated that this technology functions not only immobilized metals in a stable matrix to reduce its environmental hazard [49], but

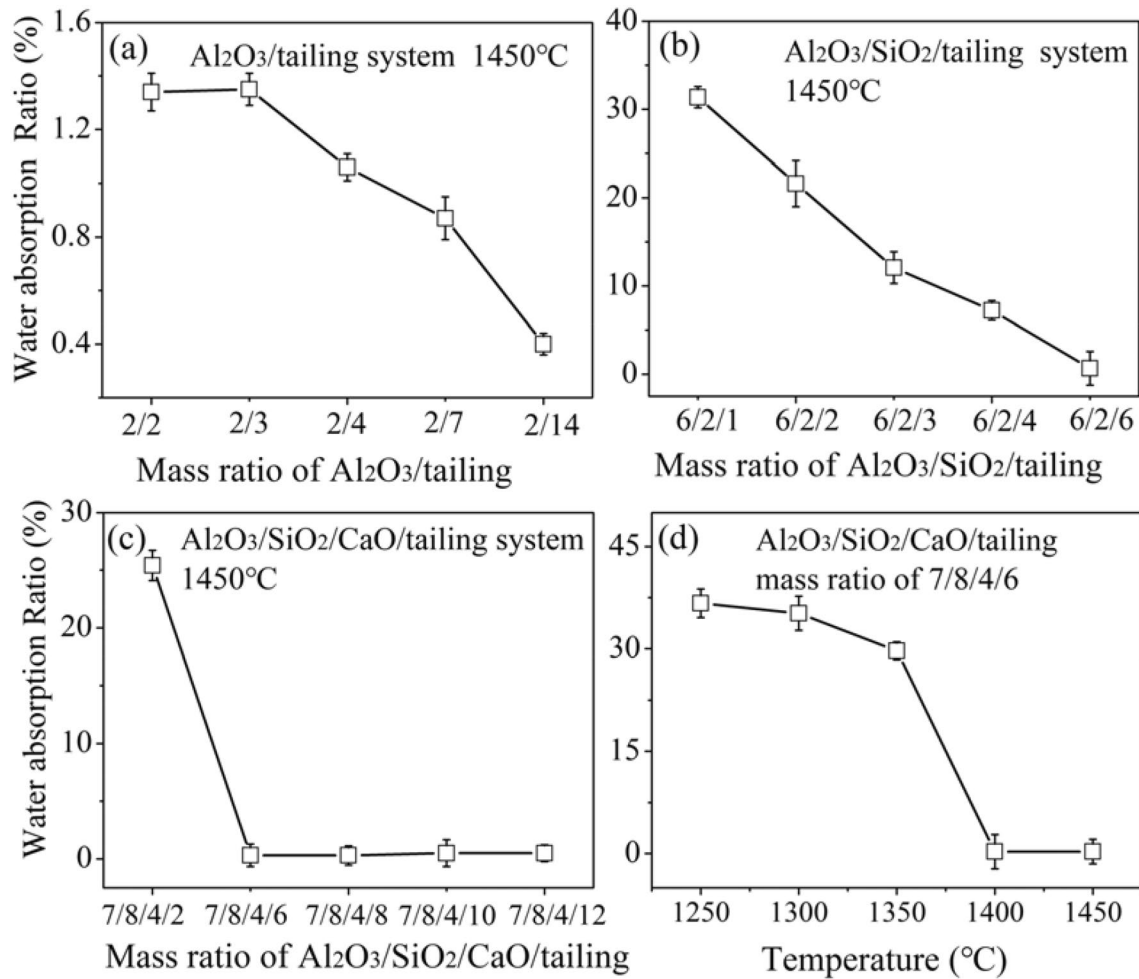


**Fig. 5** The water absorption of glass ceramics in **a**  $\text{Al}_2\text{O}_3$ /tailing system; **b**  $\text{Al}_2\text{O}_3/\text{SiO}_2$ /tailing system; **c**  $\text{Al}_2\text{O}_3/\text{SiO}_2/\text{CaO}$ /tailing system sintered at 1450 °C for 2 h; and **d** sample of  $\text{Al}_2\text{O}_3/\text{SiO}_2/\text{CaO}$ /tailing mass ratio of 7/8/4/6 sintered at 1250–1450 °C for 2 h

also provided the feasibility of reusing iron tailings as raw materials to produce glass ceramic products.

## Conclusions

Glass ceramics were successfully obtained by sintering iron tailings with  $\text{Al}_2\text{O}_3$ ,  $\text{SiO}_2$ , and  $\text{CaO}$ . Mullite was observed as the mainly crystalline phase (maximum of 72.9 wt%) in  $\text{Al}_2\text{O}_3$ /tailing and  $\text{Al}_2\text{O}_3/\text{SiO}_2$ /tailing systems, while anorthite was the newly formed crystalline phase with its maximum content of 72.9 wt% in  $\text{Al}_2\text{O}_3/\text{SiO}_2/\text{CaO}$ /tailing system. The porosity of the obtained products reduced as the addition of tailings content into

glass ceramics and the increase of sintering temperature. The obtained glass ceramics were determined with excellent chemical resistance of 79.3–99.99%, water absorption ratio of 0.2–31.3%, and compressive strength values of 170.3–1061.6 MPa, and the results are compatible to common commercial materials. By increasing content of iron tailing and sintering temperature, the glass ceramic samples with best properties were obtained for sample with  $\text{Al}_2\text{O}_3/\text{SiO}_2$ /tailing mass ratio of 6/2/6. The sample exhibited high chemical resistance of 99.99%, low water absorption ratio of 0.2%, and compressive strength values of 1061.6 MPa. The low leaching concentration of the hazardous metals from the glass ceramics makes them suitable for both architectural and construction applications.

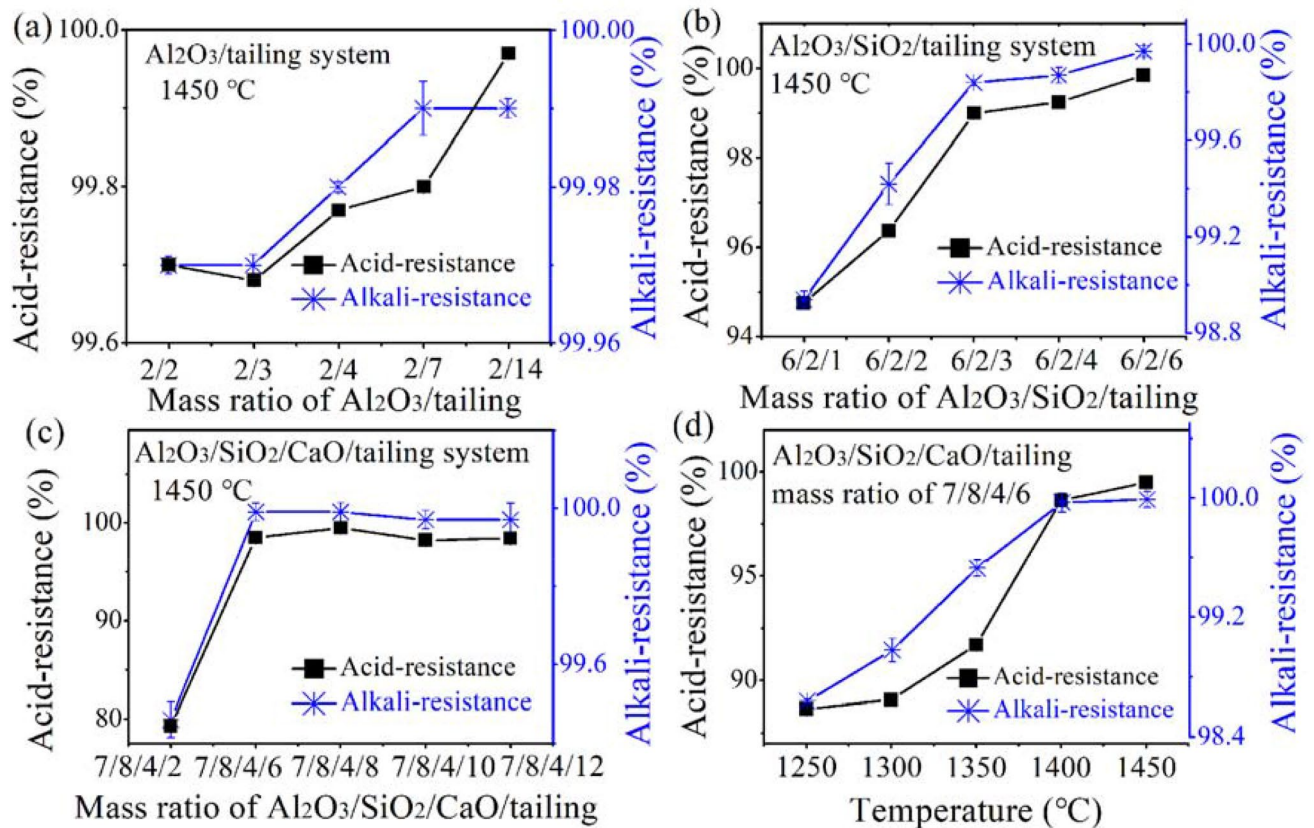


**Fig. 6** The acid and alkali resistance of glass ceramics in **a** Al<sub>2</sub>O<sub>3</sub>/tailing system; **b** Al<sub>2</sub>O<sub>3</sub>/SiO<sub>2</sub>/tailing system; **c** Al<sub>2</sub>O<sub>3</sub>/SiO<sub>2</sub>/CaO/tailing system sintered at 1450 °C for 2 h; and **d** sample of Al<sub>2</sub>O<sub>3</sub>/SiO<sub>2</sub>/CaO/tailing mass ratio of 7/8/4/6 sintered at 1250–1450 °C for 2 h

**Supplementary Information** The online version contains supplementary material available at <https://doi.org/10.1007/s40831-022-00553-5>.

**Acknowledgements** This research was supported by National Natural Science Foundation of China (22106021, 42177408), Guangdong (China) Innovative and Entrepreneurial Research Team Program (2016ZT06N258), and the Guangdong Basic and Applied Basic Research Foundation (2021A1515012372).

## Declarations

**Conflict of interest** The authors declare that they have no conflict of interest.

## References

- Ma BG, Cai LX, Li XG, Jian SW (2016) Utilization of iron tailings as substitute in autoclaved aerated concrete: physico-mechanical and microstructure of hydration products. *J Clean Prod* 127:162–171
- Li WS, Lei GY, Xu Y, Huang QF (2018) The properties and formation mechanisms of eco-friendly brick building materials fabricated from low-silicon iron ore tailings. *J Clean Prod* 204:685–692
- Cheng YH, Huang F, Li WC et al (2016) Test research on the effects of mechanochemically activated iron tailings on the compressive strength of concrete. *Constr Build Mater* 118:164–170
- Shettima AU, Hussin MW, Ahmad Y, Mirza J (2016) Evaluation of iron ore tailings as replacement for fine aggregate in concrete. *Constr Build Mater* 120:72–79
- Young G, Yang M (2019) Preparation and characterization of Portland cement clinker from iron ore tailings. *Constr Build Mater* 197:152–156
- Li J, Wang Q, Liu JH, Li P (2009) Synthesis process of forsterite refractory by iron ore tailings. *J Environ Sci* 21(S1):S92–S95
- Lv XD, Shen WG, Wang L et al (2019) A comparative study on the practical utilization of iron tailings as a complete replacement of normal aggregates in dam concrete with different gradation. *J Clean Prod* 211:704–715
- Zhao SJ, Fan JJ, Sun W (2014) Utilization of iron ore tailings as fine aggregate in ultra-high performance concrete. *Constr Build Mater* 50:540–548
- Li RF, Zhou Y, Li CW et al (2019) Recycling of industrial waste iron tailings in porous bricks with low thermal conductivity. *Constr Build Mater* 213:43–50
- da Silva FL, Araújo FGS, Teixeira MP et al (2014) Study of the recovery and recycling of tailings from the concentration of iron ore for the production of ceramic. *Ceram Int* 40(10):16085–16089
- Das SK, Kumar S, Ramachandrarao P (2000) Exploitation of iron ore tailing for the development of ceramic tiles. *Waste Manage* 20(8):725–729

12. Li C, Sun HH, Yi ZL, Li LT (2010) Innovative methodology for comprehensive utilization of iron ore tailings. *J Hazard Mater* 174(1–3):78–83
13. Yao R, Liao SY, Chen XY et al (2016) Effects of ZnO and NiO on material properties of microwave absorptive glass-ceramic tile derived from iron ore tailings. *Ceram Int* 42(7):8179–8189
14. Deng LB, Zhang XF, Zhang MX et al (2019) Structure and properties of in situ synthesized FeSi<sub>2</sub>-diopside glass ceramic composites from Bayan Obo tailings, blast furnace slag, and fly ash. *J Alloys Compd* 785:932–943
15. Xi CP, Zheng F, Xu JH et al (2018) Preparation of glass-ceramic foams using extracted titanium tailing and glass waste as raw materials. *Constr Build Mater* 190:896–909
16. Cheng JS, Kang JF, Lou XC et al (2015) Effect of TiO<sub>2</sub> on crystallization of the glass ceramics prepared from granite tailings. *J Wuhan Univ Technol* 30(1):22–26
17. Deng LB, Zhang XF, Zhang MX et al (2018) Effect of CaF<sub>2</sub> on viscosity, structure and properties of CaO-Al<sub>2</sub>O<sub>3</sub>-MgO-SiO<sub>2</sub> slag glass ceramics. *J Non-Cryst Solids* 500:310–316
18. Mukherjee DP, Das SK (2014) The influence of TiO<sub>2</sub> content on the properties of glass ceramics: crystallization, microstructure and hardness. *Ceram Int* 40(30):4127–4134
19. Liu JJ, Zou J, Guo MX, Moelans N (2018) Phase-field simulation and analytical modelling of CaSiO<sub>3</sub> growth in CaO-Al<sub>2</sub>O<sub>3</sub>-SiO<sub>2</sub> melts. *Comput Mater Sci* 144:126–132
20. Zhang WT, He F, Xiao YL et al (2019) Effects of Al/Na and heat treatment on the structure and properties of glass ceramics from molten blast furnace slag. *Ceram Int* 45(11):13692–13700
21. Liu S, Boffa V, Yang D et al (2018) Clarifying the gel-to-glass transformation in Al<sub>2</sub>O<sub>3</sub>-SiO<sub>2</sub> systems. *J Non-Cryst Solids* 492:77–83
22. Singh SP, Rodrigues AM, Orsolini HD et al (2017) Crystallization pathways and some properties of lithium disilicate oxynitride glasses. *Ceram Int* 43(15):12348–12356
23. Erol M, Küçükbayrak S, Ersoy-Meriçboyu A (2007) Production of glass-ceramics obtained from industrial wastes by means of controlled nucleation and crystallization. *Chem Eng J* 132(1–3):335–343
24. Aramaki S, Roy R (1962) Revised phase diagram for the system Al<sub>2</sub>O<sub>3</sub>-SiO<sub>2</sub>. *J Am Ceram Soc* 45:229–242
25. Liu TY, Lin CW, Liu JL et al (2018) Phase evolution, pore morphology and microstructure of glass ceramic foams derived from tailings wastes. *Ceram Int* 44(12):14393–14400
26. Zhang YF, Zhao DH, Yue YZ (2017) Phase transitions and glass transition in a hyperquenched silica-alumina glass. *J Am Ceram Soc* 100:3434–3439
27. Calligaris GA, da Silva TLT, Ribeiro APB et al (2018) On the quantitative phase analysis and amorphous content of triacylglycerols materials by X-ray Rietveld method. *Chem Phys Lipids* 212:51–60
28. Lu JS, Cong XQ, Lu ZY (2016) Influence of magnesia on sinter-crystallization, phase composition and flexural strength of sintered glass-ceramics from waste materials. *Mater Chem Phys* 174:143–149
29. Magallanes-Perdomo M, García Carrodegua RG, Pena P et al (2009) Non-isothermal devitrification study of wollastonite-tricalcium phosphate bioeutectic® glass. *Key Eng Mater* 396–398:127–130
30. Lu X, Shih K (2015) Formation of lead-aluminate ceramics: reaction mechanisms in immobilizing the simulated lead sludge. *Chemosphere* 138:156–163
31. US EPA (1998) Applicability of the toxicity characteristic leaching procedure to mineral processing wastes. <http://www.epa.gov/osw/nonhaz/industrial/special/mining/minedock/tclp/tcremand.pdf>
32. Zeng L, Sun HJ, Peng TJ, Zheng WM (2019) The sintering kinetics and properties of sintered glass-ceramics from coal fly ash of different particle size. *Results Phys* 15:102774
33. Kukukova A, Aubin J, Kresta SM (2009) A new definition of mixing and segregation: three dimensions of a key process variable. *Chem Eng Res Des* 87(4A):633–647
34. Chen H, Lin H, Zhang P et al (2021) Immobilisation of heavy metals in hazardous waste incineration residue using SiO<sub>2</sub>-Al<sub>2</sub>O<sub>3</sub>-Fe<sub>2</sub>O<sub>3</sub>-CaO glass-ceramic. *Ceram Int* 47:8468–8477
35. Khadilkar AB, Rozelle PL, Pisupati SV (2015) A study on initiation of ash agglomeration in fluidized bed gasification systems. *Fuel* 152:48–57
36. Ilic M, Cheeseman C, Sollars C, Knight J (2003) Mineralogy and microstructure of sintered lignite coal fly ash. *Fuel* 82(3):331–336
37. Sainz MA, Serrano FJ, Amigo JM et al (2000) XRD microstructural analysis of mullites obtained from kaolinite-alumina mixtures. *J Eur Ceram Soc* 20(4):403–412
38. Liu HY, Lu HX, Chen DL et al (2009) Preparation and properties of glass-ceramics derived from blast-furnace slag by a ceramic-sintering process. *Ceram Int* 35(8):3181–3184
39. Fontes WC, Franco de Carvalho JMF, Andrade LCR et al (2019) Assessment of the use potential of iron ore tailings in the manufacture of ceramic tiles: from tailings-dams to “brown porcelain.” *Constr Build Mater* 206:111–121
40. Ren X, Zhang W, Zhang Y et al (2015) Effects of Fe<sub>2</sub>O<sub>3</sub> content on microstructure and mechanical properties of CaO-Al<sub>2</sub>O<sub>3</sub>-SiO<sub>2</sub> system. *Trans Nonferrous Met Soc China* 25:137–145
41. Peng K, Lv CZ, Yang HM (2014) Novel preparation of glass ceramics from amorphized tungsten tailings. *Ceram Int* 40(7):10291–10296
42. Liu TY, Tang Y, Han L et al (2017) Recycling of harmful waste lead-zinc mine tailings and fly ash for preparation of inorganic porous ceramics. *Ceram Int* 43(6):4910–4918
43. Zheng WM, Sun HJ, Peng TJ, Zeng L (2019) Thermal process and mechanism of phase transition and detoxification of glass-ceramics from asbestos tailings. *J Non-Cryst Solids* 517:26–31
44. Vu DH, Wang KS, Chen JH, Nam BX, Bac BH (2012) Glass-ceramic from mixtures of bottom ash and fly ash. *Waste Manage* 32(12):2306–2314
45. Yang M, Guo ZX, Deng YS et al (2012) Preparation of CaO-Al<sub>2</sub>O<sub>3</sub>-SiO<sub>2</sub> glass ceramics from coal gangue. *Int J Miner Process* 102–103:112–115
46. Li B, Guo Y, Fang J (2021) Effect of MgO addition on crystallization, microstructure and properties of glass-ceramics prepared from solid wastes. *J Alloys Compd* 881:159821
47. Ricco P, Ramos NDC, Campos TMB et al (2021) The roles of microstructure and surface energy on subcritical crack growth in glass-ceramics. *Ceram Int* 47:6827–6833
48. Toya T, Kameshima Y, Nakajima A et al (2016) Preparation and properties of glass-ceramics from kaolin clay refining waste (Kira) and paper sludge ash. *Ceram Int* 32:789–796
49. Wang GW, Ning XA, Lu XW et al (2019) Effect of sintering temperature on mineral composition and heavy metals mobility in tailings bricks. *Waste Manage* 93:112–121

**Publisher's Note** Springer Nature remains neutral with regard to jurisdictional claims in published maps and institutional affiliations.

## Authors and Affiliations

Xingwen Lu<sup>1</sup> · Ceng Zhou<sup>1</sup> · Yuxin Liu<sup>1</sup> · Yujie Wang<sup>1</sup> · Fei Wang<sup>2</sup>

<sup>1</sup> School of Environmental Science and Engineering,  
and Institute of Environmental Health and Pollution Control,  
Guangdong University of Technology, Guangzhou 510006,  
China

<sup>2</sup> School of Environment, Guangdong Key Laboratory  
of Environmental Pollution and Health, Jinan University,  
Guangzhou 510632, China